Dalton Transactions

ROYAL SOCIETY OF CHEMISTRY

PAPER

View Article Online
View Journal | View Issue

Cite this: *Dalton Trans.*, 2022, **51**, 7294

Digging into protein metalation differences triggered by fluorine containing-dirhodium tetracarboxylate analogues†

Domenico Loreto, [a] Anna Esposito, [b] Nicola Demitri, [c] Annalisa Guaragna [b] and Antonello Merlino *[a]

The catalytic and biological properties of dirhodium tetracarboxylates ($[Rh_2(\mu\text{-}O_2CR)_4L_2]$, L = axial ligand and R = CH_3-, CH_3CH_2-, *etc.*) largely depend on the nature of bridging carboxylate equatorial $\mu\text{-}O_2CR$ ligands, which can be easily exchanged by solvent molecules when R is CF_3 (*i.e.* $\mu\text{-}O_2CR$ is trifluoroacetate, tfa). Here, we prepared the $[Rh_2(OAc)(tfa)_3]$ compound and investigated its interaction with bovine pancreatic ribonuclease and lysozyme under the same conditions used to study the reactivity of these proteins with $[Rh_2(OAc)_4]$ and [*cis*-$Rh_2(OAc)_2(tfa)_2$]. UV-vis absorption spectroscopy and ^{19}F nuclear magnetic resonance studies indicate that $[Rh_2(OAc)(tfa)_3]$ rapidly loses tfa ligands and interacts with the proteins. Crystallographic data demonstrate that the reaction of $[Rh_2(OAc)(tfa)_3]$ with proteins can lead to products that are significantly different when compared to those obtained with $[Rh_2(OAc)_4]$ and [*cis*-$Rh_2(OAc)_2(tfa)_2$]: the dirhodium centre can bind the side chain of His residues at both axial and equatorial sites, at variance with what is found in the case of $[Rh_2(OAc)_4]$ and [*cis*-$Rh_2(OAc)_2(tfa)_2$]. These data indicate that the hydrolysis of dirhodium tetracarboxylates plays a significant role in defining their reaction with proteins allowing the formation of unexpected reaction products. These results suggest that [*cis*-$Rh_2(OAc)_2(tfa)_2$] and $[Rh_2(OAc)(tfa)_3]$ can be used to obtain different dirhodium/peptide and dirhodium/protein adducts with distinct catalytic properties and can explain the different cytotoxicity exhibited by tfa-containing dirhodium tetracarboxylates.

Received 21st March 2022,
Accepted 14th April 2022

DOI: 10.1039/d2dt00873d

rsc.li/dalton

Introduction

Dirhodium(II) paddlewheel complexes of the general formula $[Rh_2(\mu\text{-}O_2CR)_4L_2]$ (R = Me, Et, Pr, Bu, *etc.*) incorporate a Rh(II)–Rh(II) core surrounded by four bridging equatorial $\mu\text{-}O_2CR$ ligands and two axial ligands (L) which are anions, neutral molecules or solvent molecules.[1] The synthesis and reactivity of these complexes have been intensively studied in the last few years due to their singular catalytic and biological properties. Indeed, in organic synthesis they are commonly used as catalysts for a variety of reactions,[1] including carbene insertion into C–H (or C–X) bonds,[2] activation of enynes,[3] stereoselective cyclopropanations,[4] dipolar cycloadditions,[5] hydrosilylation of alkynes,[6] photochemical dihydrogen production[7] and conversion of CO_2 to HCOOH.[8]

Dirhodium carboxylates have also been used to produce stable metallopeptides and artificial metalloenzymes with fascinating catalytic properties.[9] Interestingly, these molecules are considered as potential chemotherapeutic agents and[10–13] as nitric oxide sensors[14,15] and are used in photodynamic therapy.[16,17] The cytotoxic activity of dirhodium tetracarboxylates is due to their ability to inhibit T7-RNA polymerase[18,19] or their capacity to bind DNA[20] and induce DNA damage in cells.[21]

Changes in the coordination sphere surrounding the dirhodium core result in electronic and structural variations that allow us to control and tune its reactivity and ability to inhibit transcription *in vitro*.[19] The exchange of equatorial ligands is largely facilitated by the presence of labile sacrificial groups, like trifluoroacetate (tfa).[9b,c] Tfa-containing dirhodium tetracarboxylates have been shown to interact with DNA better than its homologues and to exert greater toxicity than cisplatin.[22]

Although several studies have been carried out on the reactivity of dirhodium tetracarboxylates and tfa-containing dirho-

[a]*Department of Chemical Sciences, University of Naples Federico II, Complesso Universitario di Monte Sant'Angelo, via Cinthia 21, 80126 Naples, Italy. E-mail: antonello.merlino@unina.it*
[b]*Department of Chemical, Materials and Production Engineering, University of Naples Federico II, P.le V. Tecchio 80, 80125 Naples, Italy*
[c]*Elettra–Sincrotrone Trieste, S.S. 14 km 163.5 in Area Science Park, 34149 Trieste, Italy*

† Electronic supplementary information (ESI) available. See DOI: https://doi.org/10.1039/d2dt00873d

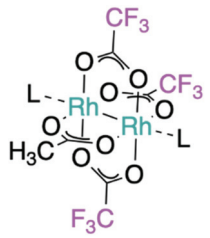

Fig. 1 Structure of the paddle-wheel compound $[Rh_2(OAc)(tfa)_3]$. Axial donor ligands (L) are shown.

dium compounds with DNA,[21,22] little is known about their interaction with proteins.

We have recently shown that *cis*-$Rh_2(\mu\text{-}O_2CCH_3)_2(\mu\text{-}O_2CCF_3)_2$ ($[cis\text{-}Rh_2(OAc)_2(tfa)_2]$) reacts with proteins[23] forming adducts that are not identical to those formed when the same proteins react with dirhodium tetraacetate ($[Rh_2(OAc)_4]$).[24,25] In particular, the reaction of $[cis\text{-}Rh_2(OAc)_2(tfa)_2]$ with the model proteins bovine pancreatic ribonuclease (RNase A) and hen egg white lysozyme (HEWL) leads to the formation of adducts with a dirhodium core that has lost all its tfa ligands.[23] The dirhodium moiety binds the side chain of His residues at the axial site. Axial protein coordination to the dirhodium centre could play a role in the binding of dirhodium tetracarboxylates to T7-RNA polymerase.[18,19,26] For this protein, Asp812, Asn748, and Glu148 have been surmised as Rh binding sites.[26] Furthermore, it has been suggested that $[Rh_2(OAc)_4]$ binds human serum albumin (HSA) *via* its axial positions in an approximately 8 : 1 dimetallic compound : protein molar ratio.[27]

To evaluate if the presence of additional tfa ligands, which facilitate the hydrolysis of the dirhodium compound, could affect the reactivity of dirhodium tetracarboxylates with proteins, the interaction of $[Rh_2(OAc)(tfa)_3]$ (Fig. 1) with RNase A and HEWL has been herein investigated in comparison with that of $[cis\text{-}Rh_2(OAc)_2(tfa)_2]$[23] and $[Rh_2(OAc)_4]$.[24,25] In particular, the product of the reaction of $[Rh_2(OAc)(tfa)_3]$ with RNase A and HEWL has been characterized using UV-vis absorption spectroscopy, circular dichroism, X-ray crystallography and ^{19}F nuclear magnetic resonance (NMR).

Methods

Materials

All starting materials and proteins were purchased from Sigma Chemical Co and used without further purification. CH_3CN and toluene of the highest commercial quality were purchased from VWR (Milan, Italy) or Merck Life Science S.r.l (Milan, Italy) and used as received.

Synthesis

$[Rh_2(OAc)(tfa)_3]$ was synthesized using a published protocol with slight modifications[23] (experimental details are reported in the ESI†). Precoated silica gel TLC plates (F254, Merck, Darmstadt, Germany) were used to check the progress of the reaction; the exposure of TLC to UV light and iodine vapor was used for monitoring of product formation. Column chromatography was performed using a 70–230 mesh silica gel sorbent (Merck Kieselgel 60). NMR spectra were recorded on a 400 MHz (Bruker AVANCE, Billerica, Massachusetts, US) or 500 MHz (Varian Inova, Palo Alto, California, US) spectrometer. The chemical shifts (δ) are expressed in ppm.

Crystallization, data collection and refinement

The crystals of the adducts formed upon the reaction of RNase A and HEWL with $[Rh_2(OAc)(tfa)_3]$ were obtained by soaking method.[28] Metal-free protein crystals were grown at 298 K using the hanging drop vapor diffusion method, using a previously reported procedure.[24,25] RNase A crystals were grown using a protein concentration of 22 mg mL^{-1} and a reservoir consisting of 22% PEG 4 K and 0.01 M sodium citrate, pH 5.1, while in the case of HEWL, a protein concentration of 18 mg mL^{-1} was used, with a reservoir consisting of 0.10 M HEPES, pH 7.5, and 2.00 M sodium formate.

Soaking was carried out using a 5.00 mM solution of $[Rh_2(OAc)(tfa)_3]$, freshly dissolved in the reservoir. The soaking time was 4 days for all the crystals.

For data collection, 20% (v/v) glycerol was added to the mother liquor solution. The crystals were then flash-cooled with liquid N_2.

Diffraction data were collected on two crystals of RNase A treated with $[Rh_2(OAc)(tfa)_3]$ and one crystal of HEWL exposed to the same compound at the XRD2 beamline of Elettra synchrotron in Trieste, Italy.[29] Data sets were reduced and merged using the Global Phasing autoPROC pipeline implemented at Elettra.[30] Data collection statistics are reported in Table 1.

The structures were solved by molecular replacement with Phaser[31] in CCP4 using reported coordinates of the structures of metal-free RNase A (chain A from PDB code 1JVT)[32] and of metal-free HEWL (PDB code 193L)[33] as search models. Model building, adjustments and visualization of the electron density maps were carried out using Coot.[34] Refinements were carried out using Refmac5.[35] Rh centre positions were identified by analyzing Fourier difference and anomalous difference electron density maps. Metal and ligand occupancies were evaluated by minimizing the positive and negative peaks on the metal centre in the Fourier difference electron density maps. The quality of the final models was evaluated using the PDB validation server.[36] The refinement of the final model was also carried out using Phenix for a software comparison,[37] as suggested by Brink and Helliwell.[38] Atomic coordinates and structural factors for the reported structures have been deposited in the Protein Data Bank as entries 7Z6D and 7Z6G for the Rh/RNase A adducts, and 7Z6J for the Rh/HEWL adduct. These data were made available to editors and peer reviewers during the review process. All structural figures were generated using PyMOL (**https://www.pymol.org**). A list of uninterpreted peaks in the Fourier difference electron density map is reported in Table S1,† as previously determined by us[23,39] and other authors.[40]

Table 1 Data collection and refinement statistics

Protein	RNase A Crystal **1**	RNase A Crystal **2**	HEWL
PDB code	7Z6D	7Z6G	7Z6J
Crystallization conditions	22% PEG 4 K, 10 mM sodium citrate at pH 5.1		10 mM HEPES pH 7.5 and 2.00 M sodium formate
Data collection			
Space group	*C*2	*C*2	$P4_32_12$
a (Å)	101.18	100.12	78.55
b (Å)	32.95	32.41	78.59
c (Å)	73.28	72.27	37.39
β (°)	90.17	90.44	90.01
Resolution range (Å)	50.85–1.45 (1.48–1.45)	30.99–1.71 (1.74–1.71)	39.31–1.53 (1.56–1.53)
Unique reflections	43 428 (2151)	25 642 (1242)	18 041 (899)
Completeness (%)	99.0 (100.0)	99.9 (100.0)	98.8 (100.0)
Redundancy	5.2 (5.6)	6.3 (6.2)	23.3 (25.1)
R_{merge}[a] (%)	0.185 (0.796)	0.079 (0.795)	0.052 (1.749)
R_{pim}	0.135 (0.557)	0.052 (0.521)	0.015 (0.500)
Average $I/\sigma(I)$	11.8 (3.1)	12.5 (2.2)	32.1 (2.1)
$CC_{1/2}$	0.998 (0.670)	0.997 (0.782)	1.000 (0.752)
ANOM. completeness (%)	97.9 (99.4)	99.5 (99.7)	98.9 (100.0)
ANOM. Redundancy	2.7 (2.9)	3.3 (3.2)	12.6 (13.2)
Refinement			
Asymmetric unit content	Two protein molecules	Two protein molecules	One protein molecule
Resolution range (Å)	50.85–1.45	30.99–1.71	39.31–1.53
N. of reflections	41 357	24 495	17 071
N. of reflections (test set)	3054	1755	1218
R-factor/R-free (%)	20.1/23.2	18.3/23.6	19.5/24.8
N. of atoms	2365	2207	1240
Average B-factors (Å^2)			
All atoms	19.1	26.9	27.3
Rh atoms[b]	30.7/38.9/36.4/44.2 22.9/25.2/26.9/28.1	35.7/57.0/52.1/68.0 34.2/41.1/45.2/56.1	61.2/59.8/58.7/54.7/47.9
Rh occupancy	0.50/0.50/0.40/0.40 0.20/0.20/0.40/0.40	0.70/0.70/0.55/0.55 0.30/0.30/0.55/0.55	0.25/0.25/0.30/0.25/0.30
R.m.s. deviations			
Bond lengths (Å)	0.013	0.011	0.010
Bond angles (°)	1.83	2.22	1.74
Ramachandran statistics (Coot analysis)			
No. of residues in allowed/disallowed regions	9/3	7/4	6/0

[a] $R_{merge} = \sum h \sum i |I(h,i) - \langle I(h)\rangle| / \sum h \sum i\, I(h,i)$, where $I(h,i)$ is the intensity of the i^{th} measurement of reflection h and $\langle I(h)\rangle$ is the mean value of the intensity of reflection h. [b] As expected, Rh atoms bound to His residues have a lower B-factor than their Rh partner.

UV-vis absorption spectroscopy and circular dichroism

To analyze the chemical environment of $[Rh_2(OAc)(tfa)_3]$ in aqueous medium, UV–vis absorption spectra were recorded at room temperature in the 340–720 nm range. The spectra of the metal complex (0.5 mM) were recorded on a Jasco V750 UV–vis spectrophotometer in 10.0 mM sodium citrate, pH 5.1, and in 5.0 mM HEPES, pH 7.5, in the absence and presence of RNase A and HEWL, respectively (protein to metal molar ratio of 1 : 3).

The circular dichroism (CD) spectra of RNase A and HEWL in the absence and presence of $[Rh_2(OAc)(tfa)_3]$ were recorded upon 24 h incubation in the far-UV region (from 200 to 250 nm) using a Jasco J-810 spectropolarimeter (JASCO Corp., Milan, Italy) at 25 °C. Samples were obtained by incubating the proteins with $[Rh_2(OAc)(tfa)_3]$ at a 1 : 3 molar ratio in 10.0 mM sodium citrate buffer at pH 5.1 and in 5.0 mM HEPES at pH 7.5 in the case of RNase A and HEWL, respectively. Ellipticity is reported as molar ellipticity per mean residue in ([θ] deg cm^2 dmol^{-1}) and calculated from the equation: $[\theta] = [\theta]_{obs}\cdot mrw/10lC$, where $[\theta]_{obs}$ is the ellipticity measured in degrees, mrw is the mean residue molecular weight, C is the protein concentration in g ml^{-1} and l is the optical path length of the cell in cm. The following parameters were used: 0.1 cm path length, 50 nm min^{-1} scan speed, 2.0 nm bandwidth, 0.2 nm resolution, 50 mdeg sensitivity, and 4 s response. Spectra were signal-averaged over three scans, subtracting contributions from the corresponding references.

^{19}F nuclear magnetic resonance

A Bruker AVANCE spectrometer (Billerica, Massachusetts, US) operating at 376 MHz was used to acquire ^{19}F NMR spectra (25 °C), using TOPSPIN as the software interface. 10.0 mM sodium citrate, pH 5.1, and 5.0 mM HEPES, pH 7.5 (10% D_2O), solutions were used to obtain a 0.5 mM solution of the metal complex in the absence and presence of the proteins (in a 1 : 1 protein to metal compound molar ratio). The same buffer solutions (10.0 mM sodium citrate and 10% D_2O at pH 5.1 and 5.0 mM HEPES and 10% D_2O at pH 7.5) were used to obtain the reference spectra of the pure TFA.

Results

Synthesis and characterization of $[Rh_2(OAc)(tfa)_3]$

To synthesize the $[Rh_2(OAc)(tfa)_3]$ dirhodium complex, the same protocol already described to prepare the [*cis*-$Rh_2(OAc)_2(tfa)_2$] complex was used by slightly modifying the reaction time.[23] In particular, dirhodium tetraacetate $[Rh_2(OAc)_4]$ was treated with an excess of trifluoroacetic acid (TFA), at room temperature, to give, after 6 h, the $[Rh_2(OAc)(tfa)_3]$ compound in a good yield (55%) as a blue powder. ^1H and ^{19}F NMR data were in agreement with the literature values (see ESI Fig. S1†).[41]

Stability of $[Rh_2(OAc)(tfa)_3]$ in aqueous solution and in solution reactivity with proteins

Its stability in aqueous solution and reactivity with RNase A and HEWL were investigated by UV-vis absorption spectroscopy, ^{19}F NMR spectroscopy and circular dichroism, under the same conditions used to obtain crystals of the two proteins (10.0 mM sodium citrate buffer, pH 5.1, and 5.0 mM HEPES solution, pH 7.5) and using the same protocol developed to study the stability of $[Rh_2(OAc)_4]$[24,25] and [*cis*-$Rh_2(OAc)_2(tfa)_2$][23] under the same conditions.

In sodium citrate at pH 5.1, the UV-vis absorption spectrum of $[Rh_2(OAc)(tfa)_3]$ shows two bands in the visible region, at λ_{max} = 458 nm (band I, assigned to $Rh_2(\pi^*) \rightarrow Rh–O(\sigma^*)$ transitions) and at 583 nm (band II, assigned to the $Rh_2(\pi^*) \rightarrow Rh_2(\sigma^*)$ transition of the metal–metal single bond), respectively (Fig. 2A).

As observed in the case of [*cis*-$Rh_2(OAc)_2(tfa)_2$],[23] the UV-vis spectra of $[Rh_2(OAc)(tfa)_3]$ as a function of time reveal the stability of the complex for three hours and significant changes of the spectral profile after 24 h. In particular, a blue-shift of band I from its initial λ_{max} up to 407 nm and a small red-shift of band II from 583 nm to 588 nm were observed. These results suggest that the compound retains the dirhodium centre but exchanges its equatorial ligands with solvent molecules over time. In this respect, it is useful to note that after 24 h the spectrum of $[Rh_2(OAc)(tfa)_3]$ is significantly different when compared to that observed in the case of [*cis*-$Rh_2(OAc)_2(tfa)_2$]. Indeed, the spectrum of the *cis* compound reveals a clear signal at 444 nm, while in that of $[Rh_2(OAc)(tfa)_3]$ a broad signal for band I is found. This difference could be related to the finding that after the hydrolysis of $[Rh_2(OAc)(tfa)_3]$, different products can be formed (see Scheme S2†).

In the presence of RNase A (Fig. 2B), the UV-vis spectrum of $[Rh_2(OAc)(tfa)_3]$ changes more rapidly than in the absence of the protein. Even at t = 0 min, band I was not observed. Furthermore, a red-shift of band II was found, with the λ_{max} changing from 566 nm to 580 nm over 24 h.

These results suggest that $[Rh_2(OAc)(tfa)_3]$ instantaneously exchanges almost all its tfa ligands in the presence of the protein and the exchange does not significantly alter the dimetallic bond.

The electronic spectrum of $[Rh_2(OAc)(tfa)_3]$ in 5.0 mM HEPES buffer at pH 7.5 shows the bands I (at λ_{max} = 458 nm) and II (at λ_{max} = 581 nm), assigned to $Rh_2(\pi^*) \rightarrow Rh–O(\sigma^*)$ transitions and to the $Rh_2(\pi^*) \rightarrow Rh_2(\sigma^*)$ transition of the metal–metal single bond (Fig. 3A). Band I disappears just after 30 min, suggesting that a rapid release of tfa ligands occurs also under these experimental conditions. Furthermore, a blue-shift of band II from λ_{max} = 581 nm to 571 nm was observed. In the presence of the protein, at t = 0, *i.e.* just after the addition of HEWL, band I was not observed, suggesting an almost complete release of tfa ligands from the dirhodium core. In contrast, band II shows a red-shift from 568 to 575 nm, as observed in the case of [*cis*-$Rh_2(OAc)_2(tfa)_2$] under the same experimental conditions (Fig. 3B).

To obtain further experimental evidence of the rapid exchange of tfa ligands from the dirhodium unit and the potential interaction with proteins, the ^{19}F NMR spectra of $[Rh_2(OAc)(tfa)_3]$ were registered over time in the absence and presence of RNase A (Fig. 4A) and HEWL (Fig. 4B) in 10.0 mM sodium citrate at pH 5.1 and 5.0 mM HEPES at pH 7.5, respectively. Data collected in citrate buffer reveal that, after 5 min, the percentage of tfa ligands that is lost by $[Rh_2(OAc)(tfa)_3]$ is higher when compared to that by [*cis*-$Rh_2(OAc)_2(tfa)_2$] (see Fig. 3A in ref. 23). In the spectrum of $[Rh_2(OAc)(tfa)_3]$ collected under these conditions, several peaks were observed and they

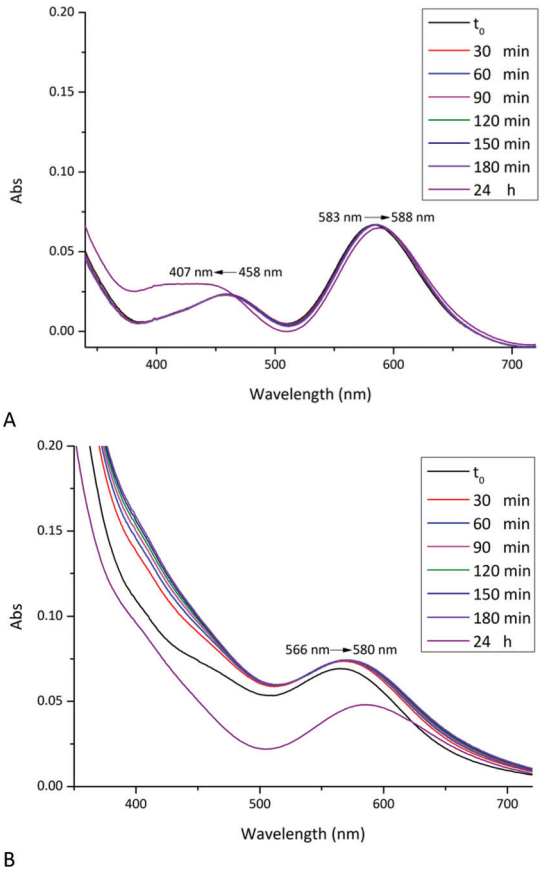

Fig. 2 Temporal evolution of the UV-vis spectra of $[Rh_2(OAc)(tfa)_3]$ in 10.0 mM sodium citrate buffer at pH 5.1 in the absence (panel A) and presence (panel B) of RNase A (protein to metal molar ratio: 1 : 3).

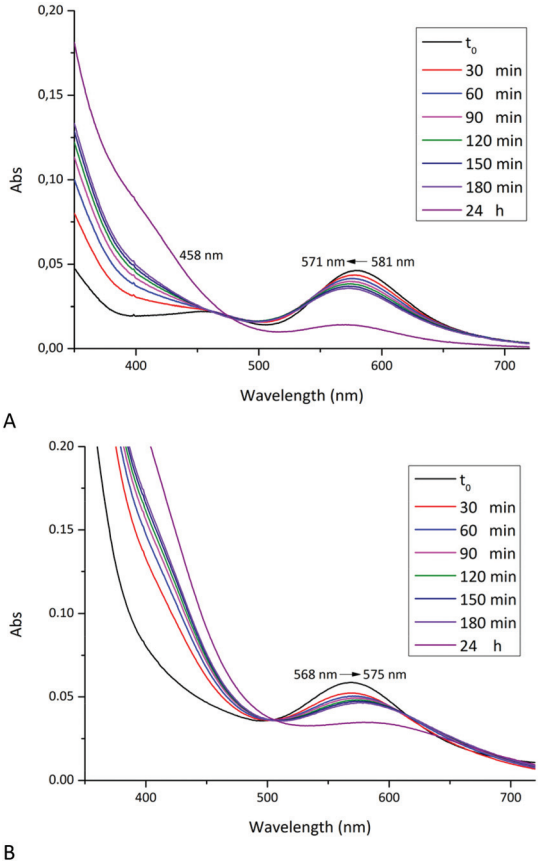

Fig. 3 Temporal evolution of UV-vis absorption spectra of $[Rh_2(OAc)(tfa)_3]$ in 5.0 mM HEPES at pH 7.5 in the absence (panel A) and presence (panel B) of HEWL (protein to metal molar ratio: 1 : 3).

could be associated with the different products of the hydrolysis of the compound when compared to that of [*cis*-$Rh_2(OAc)_2(tfa)_2$]. At 24 h, as observed in the case of [*cis*-$Rh_2(OAc)_2(tfa)_2$], $[Rh_2(OAc)(tfa)_3]$ loses almost all its tfa ligands. Notably, in the presence of RNase A, the hydrolysis of the compound is almost instantaneous since the complete release of tfa ligands was observed just after the addition of the protein. In HEPES buffer, the comparison of the spectra collected over time suggests that a mixture of species exists after 24 h. In contrast, data collected in the presence of HEWL indicate a complete release of tfa from the dirhodium compound after 2 hours. Overall, these results suggest that, like its parent compounds $[Rh_2(OAc)_4]$[24,25] and [*cis*-$Rh_2(OAc)_2(tfa)_2$],[23] $[Rh_2(OAc)(tfa)_3]$ binds both RNase A and HEWL, in agreement with the indications derived from the comparison of the electronic spectra of the compound registered in the absence and presence of the proteins, and that hydrolyzed species are those interacting with the proteins.

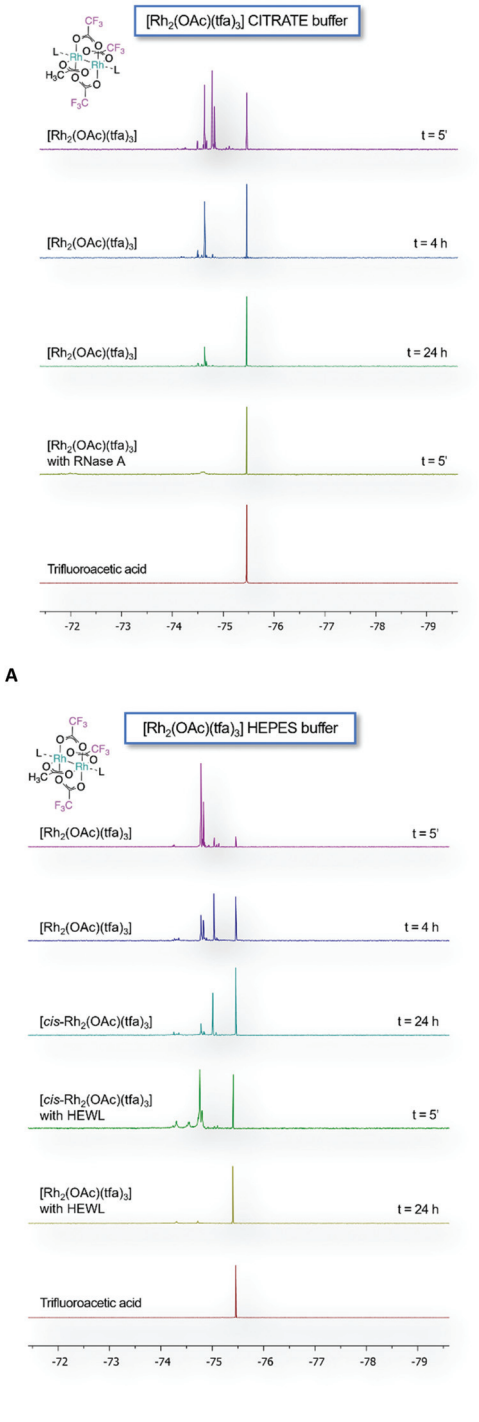

Fig. 4 Time course ^{19}F NMR spectra of $[Rh_2(OAc)(tfa)_3]$ in 10.0 mM sodium citrate buffer at pH 5.1 (10% D_2O) in the absence and presence of RNase A (protein to metal ratio 1 : 1) (panel A), and in 5.0 mM HEPES buffer at pH 7.5 (10% D_2O) in the absence and presence of HEWL (protein to metal molar ratio: 1 : 1) (panel B).

Effect of $[Rh_2(OAc)(tfa)_3]$ binding to proteins in solution

To compare the structures of the proteins in solution, in the absence and presence of $[Rh_2(OAc)(tfa)_3]$, CD measurements were performed (Fig. 5). Far-UV CD spectra of metal-free RNase A and HEWL and the proteins incubated for 24 h with $[Rh_2(OAc)(tfa)_3]$ in a 1 : 3 protein/metal compound molar ratio have a similar shape and compare well with the literature data.[23,25] This finding strongly indicates that the proteins

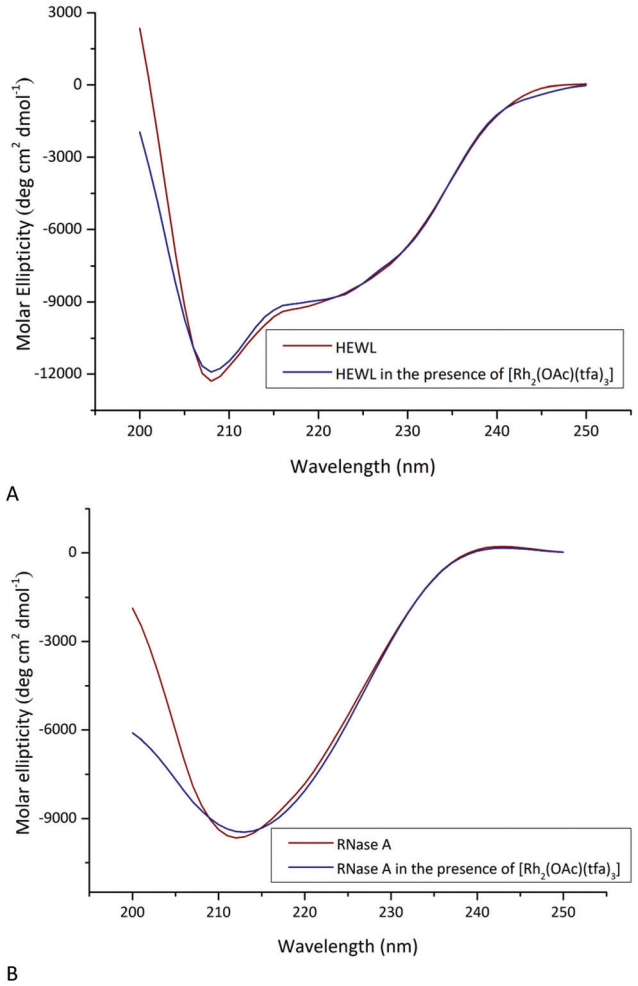

Fig. 5 Far-UV CD spectra of (A) HEWL in 5.0 mM HEPES buffer at pH 7.5 in the absence and presence of $[Rh_2(OAc)(tfa)_3]$ in a 1 : 3 protein to metal molar ratio and (B) RNase A in 10.0 mM sodium citrate buffer at pH 5.1 in the absence and presence of $[Rh_2(OAc)(tfa)_3]$ in a 1 : 3 protein to metal molar ratio. Spectra were registered after 24 h of incubation.

retain their folded conformation and have almost the same content of secondary structure in the presence of a metal compound, in agreement with what was observed for the adducts formed upon the reaction of the two proteins with $[Rh_2(OAc)_4]$[25] and [*cis*-$Rh_2(OAc)_2(tfa)_2$].[23]

Interaction of $[Rh_2(OAc)(tfa)_3]$ with RNase A

In order to unveil which is the product of the reaction between $[Rh_2(OAc)(tfa)_3]$ and RNase A, two structures derived from the crystals of the protein treated with the Rh compound have been refined at 1.45 to 1.71 Å resolution. Since the results of the two structural determinations are similar, only data at higher resolution are discussed. To obtain the crystals of the adduct, the soaking strategy was chosen, since in this way, the results obtained with $[Rh_2(OAc)(tfa)_3]$ could be strictly compared to those found with [*cis*-$Rh_2(OAc)_2(tfa)_2$][23] and $[Rh_2(OAc)_4]$.[24] Metal binding sites were found close to the side chain of His105 of molecule A and to the side chains of His119

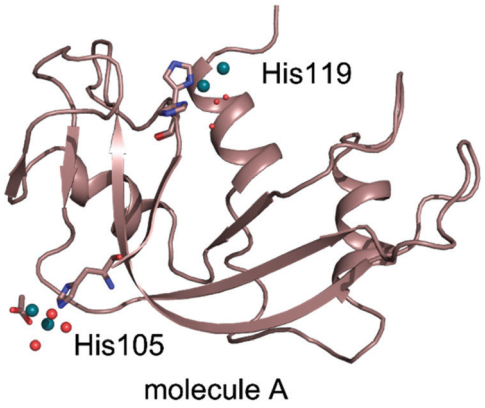

Fig. 6 Overall structure of the Rh/RNase A adduct formed in the reaction of the protein with $[Rh_2(OAc)(tfa)_3]$ (molecule A of the monoclinic crystal form with two molecules in the asymmetric unit). Rh atoms are shown in dark green. The asymmetric unit content and an image of molecule B are reported in the ESI.†

of both molecules A and B of RNase A in the studied monoclinic crystal form with two molecules (A and B) in the asymmetric unit (Fig. 6 and Fig. S2 and S4†). His105 and His119 have been already identified as metal binding sites in previous works.[42–45] In particular, the side chains of these residues can bind Pt[39,42] and references therein, Ir,[43] Au,[42b,44] and Ru.[45]

The three-dimensional structures of molecules A and B closely resemble the RNase A structures in the adducts with [*cis*-$Rh_2(OAc)_2(tfa)_2$][23] and $[Rh_2(OAc)_4]$.[24] After superposition, the 124 Cα atoms of molecules A and B have root-mean-square (r.m.s.) deviations within the range of 0.099–0.448 Å (Table S2†).

Consistent with ^{19}F NMR data, diffraction data indicate that dirhodium cores lose all their original tfa ligands. In all the dirhodium binding sites, the dimetallic core is well defined, while in many cases, its ligands are not well defined in electron density maps.

In the protein active site of molecule A, the side chain of His119 adopts two different conformations, which are both compatible with the binding to the dirhodium centre, one at the axial (distance between N of imidazole and Rh = 2.28 Å) and the other at the equatorial site (distance between N of imidazole and Rh = 2.19 Å) (Fig. 7A and Fig. S4A†). In molecule B, His119 also adopts two different conformations. However, in this case, both the His conformations bind dirhodium centres at the axial site (Fig. 7B and Fig. S4B†). In this site, the interpretation of the e.d. map is complicated by the finding that two dirhodium centres are close to each other. However, our model is supported by the finding that we have two structures with very similar results. The distances between Rh atoms at this site are 2.29 and 2.17 Å. Additional evidence of the possibility that the dirhodium centre can bind RNase A also equatorially, at variance with [*cis*-$Rh_2(OAc)_2(tfa)_2$][23] and $[Rh_2(OAc)_4]$,[24] comes from the observation of the electron density map close to the side chain of His105 of molecule A. Here, a dirhodium centre equatorially coordinated to the

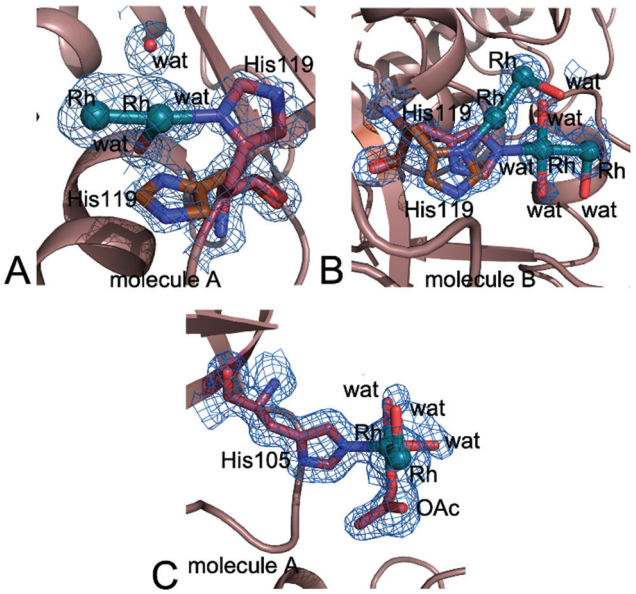

Fig. 7 The dirhodium core binding site close to (A) His119 of molecule A and (B) His119 of molecule B. (C) His105 of molecule A in the structure of the adduct formed upon the reaction of RNase A with $[Rh_2(OAc)(tfa)_3]$. 2Fo–Fc electron density maps are contoured at 1.0σ in panels A and B and at 0.8σ in panel C.

imidazole of the residue side chain, with water molecules as ligands, was clearly observed (Fig. 7C and Fig. S4C†). At this site, close to the dirhodium centre, an acetate ligand, coordinated to only one Rh centre was found. The coordination sphere of the dirhodium centre is not completely defined in the electron density map. These data demonstrate that $[Rh_2(OAc)(tfa)_3]$ loses all its tfa ligands before the acetate and that the His side chain can coordinate to the dirhodium centre at the equatorial site.

Metals were not observed close to the side chain of His105 in molecule B.

A summary of the dirhodium ligands and of geometries of the dirhodium compound fragments observed in the present structure(s) is reported in Tables S3 and S4,† compared to the results obtained for the same protein with $[Rh_2(OAc)_4]$[24,25] and $[cis\text{-}Rh_2(OAc)_2(tfa)_2]$.[23]

Altogether these data support the hypothesis that $[Rh_2(OAc)(tfa)_3]$ can bind proteins at both the equatorial and axial sites, in contrast to $[Rh_2(OAc)_4]$[24,25] and $[cis\text{-}Rh_2(OAc)_2(tfa)_2]$.[23]

X-ray structures of the adduct with HEWL

The structures of the adducts formed upon the reaction of HEWL with $[Rh_2(OAc)_4]$[25] and $[cis\text{-}Rh_2(OAc)_2(tfa)_2]$,[23] obtained by treating protein crystals grown in HEPES with the Rh compounds, have shown that the dirhodium centre can degrade under these experimental conditions and that both dirhodium and monometallic centres can bind protein residue side chains. The structure of the adduct of HEWL with $[Rh_2(OAc)(tfa)_3]$, which has been refined at 1.53 Å resolution, presents results that are similar to those found in the case of $[Rh_2(OAc)_4]$[25] and $[cis\text{-}Rh_2(OAc)_2(tfa)_2]$[23] (Fig. 8). Rh binding was observed close to the side chains of His15 (Fig. 9A), Lys33 (Fig. 9B), and Asp101 (Fig. 9C), and to the C-terminal tail (Fig. 9D).

Close to the His15 side chain, a dirhodium centre (occupancy = 0.25, B-factor of Rh atoms = 60.2–62.8 Å^2) was observed (Fig. 9A). At this binding site, metal ligands were not observed in the difference Fourier electron density map and the peaks in the anomalous difference electron density maps corresponding to metal atoms were very low. The side chain of His15 was frequently identified as a metal binding site in protein metalation studies. In particular, it has been shown that this residue can bind Ru,[46] Au,[47] Ag,[48] Pt,[49] Ir[50] and Re.[51]

An additional metal centre was found close to the side chain of Lys33 (occupancy = 0.25). Here, a single metal centre

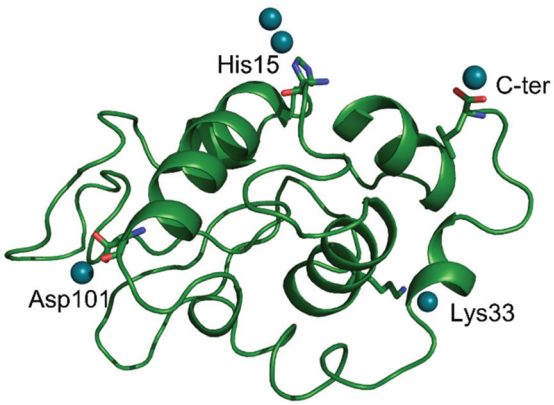

Fig. 8 Overall structure of the adduct formed upon the reaction of $[Rh_2(OAc)(tfa)_3]$ with HEWL. Rh atoms are shown in dark green.

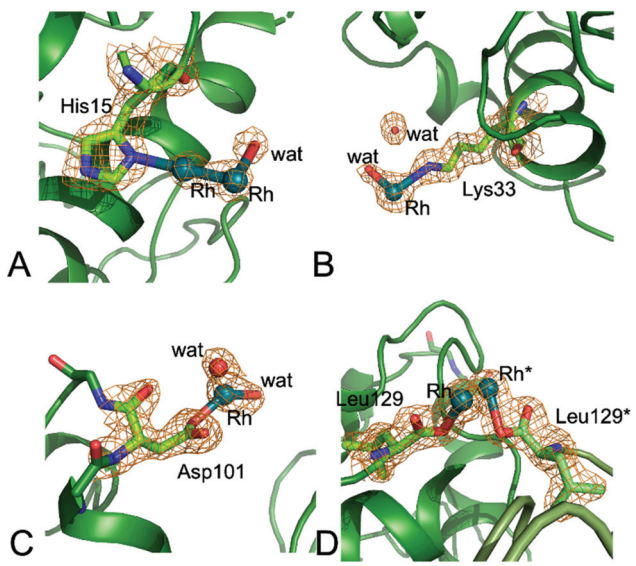

Fig. 9 Details of the Rh binding site close to (A) His15, (B) Lys33, (C) Asp101 and (D) at the C-terminal tail in the structure of the Rh/HEWL adduct obtained upon the reaction of the protein with $[Rh_2(OAc)(tfa)_3]$. * indicates residues from symmetry mates. 2Fo–Fc electron density maps are contoured at 1.0σ.

was modelled in the electron density map, although it cannot be excluded that the dirhodium centre can be bound at this site equatorially (Fig. 9B). The side chain of Lys33 can bind Ru[52] and Pt centres.[39]

One Rh centre (occupancy = 0.30) was also found close to the side chain of Asp101 (the distance between the Rh centre and the OD1 atom of Asp101 is 2.22 Å (Fig. 9C)) and to the C-terminal tail (at 2.38 Å and 2.42 Å from the oxygen atoms of the carboxylate of Leu129 and at 2.64 Å from the NZ atom of Lys13) (Fig. 9D), suggesting a significant degradation of the dirhodium compound (Rh–Rh distance of 2.79 Å). Both Asp101 and the C-terminal tail have been already shown as potential metal binding sites. Asp101 can bind Pt[42a] and Ru,[53] while the C-terminal tail has been found to be linked to Pt[39,54] and Ru.[53c]

Conclusions

The reactions of peptides and proteins with dirhodium tetracarboxylates are important not only since they affect the biological properties of the metal compounds, but also since they are used to build new artificial metallopeptides/metalloenzymes with notable catalytic properties.[9] The replacement of equatorial carboxylate ligands, surrounding the dirhodium core of dirhodium tetracarboxylates, with tfa facilitates these reactions. It has been shown that [*cis*-$Rh_2(OAc)_2(tfa)_2$] can react with proteins producing adducts with the dirhodium centre losing tfa ligands. Dirhodium containing fragments bind His side chains at the axial sites.[23] Here, we have compared the protein binding properties of [$Rh_2(OAc)(tfa)_3$] with those of [*cis*-$Rh_2(OAc)_2(tfa)_2$] and [$Rh_2(OAc)_4$].

[$Rh_2(OAc)(tfa)_3$] loses its tfa ligands just after the addition of RNase A to its solution and after 2 hours in the presence of HEWL. Crystallographic data indicate that this Rh compound can bind proteins coordinating to the His side chain at both the axial and equatorial sites, at variance with what was observed in the case of [$Rh_2(OAc)_4$][24] and [*cis*-$Rh_2(OAc)_2(tfa)_2$].[23] The binding does not alter the overall conformation of the proteins. The binding of N-containing ligands, like tert-butyl isocyanide and pyridine, to both axial and equatorial sites of the dirhodium centre has been reported by Drago *et al.*, who studied the reaction of these molecules with [$Rh_2(tfa)_4$].[55] Similar results have been obtained when binuclear molybdenum trifluoroacetate reacts with an excess of pyridine.[56] In this case, it has been surmised that the equatorial binding occurs after initial coordination at the axial position by an incoming group, followed by a dissociative ring opening of the leaving group.[55] This type of reaction product cannot be observed upon the reaction of peptides and proteins with [$Rh_2(OAc)_4$].[9,23–25,55]

Overall, these results demonstrate that [$Rh_2(OAc)_4$], [*cis*-$Rh_2(OAc)_2(tfa)_2$] and [$Rh_2(OAc)(tfa)_3$] can react with peptides and proteins producing different reaction products. This information could explain the different results obtained by studying analogous dirhodium carboxylates in their reaction with T7-RNA polymerase.[14] Data are also significant because they support the idea that dirhodium complexes can be tuned, by changing the equatorial ligands, to direct their effects on specific cellular targets. Our results suggest that different dirhodium tetracarboxylates can be used to prepare various artificial metalloenzymes with distinct properties.

Conflicts of interest

Nothing to declare.

Acknowledgements

The authors thank Elettra staff for technical assistance.

Notes and references

1 R. Hrdina, Dirhodium(II,II) Paddlewheel Complexes, *Eur. J. Inorg. Chem.*, 2021, **6**, 501–528.
2 M. P. Doyle, R. Duffy, M. Ratnikov and L. Zhou, Catalytic Carbene Insertion into C–H Bonds, *Chem. Rev.*, 2010, **110**, 704–724.
3 K. Ota, S. I. Lee, J. M. Tang, M. Takachi, H. Nakai, T. Morimoto, H. Sakurai, K. Kataoka and N. Chatani, Rh (II)-Catalyzed skeletal reorganization of 1,6- and 1,7-enynes through electrophilic activation of alkynes, *J. Am. Chem. Soc.*, 2009, **131**, 15203–15211.
4 H. Lebel, J.-F. Marcoux, C. Molinaro and A. B. Charette, Stereoselective Cyclopropanation Reactions, *Chem. Rev.*, 2003, **103**(4), 977–1050.
5 X. C. Wang, C. Weigl and M. P. Doyle, Solvent enhancement of reaction selectivity: a unique property of cationic chiral dirhodium carboxamidates, *J. Am. Chem. Soc.*, 2011, **133**, 9572–9579.
6 (*a*) M. P. Doyle, K. G. High, C. L. Nesloney, T. W. Clayton Jr. and J. Lin, Rhodium(II) Perfluorobutyrate Catalyzed Hydrosilylation of 1-alkynes. Trans Addition and Rearrangement to Allylsilanes, *Organometallics*, 1991, **10**, 1225–1126; (*b*) M. P. Doyle, G. A. Devora, A. O. Nefedov and K. G. High, Addition/elimination in the Rhodium(II) Perfluorobutyrate Catalyzed Hydrosilylation of 1-Alkenes. Rhodium Hydride Promoted Isomerization and Hydrogenation, *Organometallics*, 1992, **11**, 549–555.
7 (*a*) J. Huang, C. J. Gallucci and C. Turro, Panchromatic Dirhodium Photocatalysts for Dihydrogen Generation with Red Light, *Chem. Sci.*, 2020, **11**, 9775–9783; (*b*) H. J. Sayre, A. Millet, K. R. Dunbar and C. Turro, Photocatalytic H_2 Production by Dirhodium(II,II) Photosensitizers with Red Light, *Chem. Commun.*, 2018, **54**, 8332–8334; (*c*) J. Xie, C. Li, Q. Zhou, W. Wang, Y. Hou, B. Zhang and X. Wang, Large Improvement in the Catalytic Activity Due to Small Changes in the Diimine Ligands: New Mechanistic Insight into the Dirhodium(II,II) Complex-Based Photocatalytic H_2 Production, *Inorg. Chem.*, 2012, **51**(11), 6376–6384.

8 (*a*) H. D. Manamperi, S. E. Witt and C. Turro, Selective Electrocatalytic Conversion of CO_2 to HCOOH by a Cationic Rh_2(II,II) Complex, *ACS Appl. Energy Mater.*, 2019, **2**, 7306–7314; (*b*) S. E. Witt, T. A. White, Z. Li, K. R. Dunbar and C. Turro, Cationic Dirhodium(II,II) Complexes for the Electrocatalytic Reduction of CO_2 to HCOOH, *Chem. Commun.*, 2016, **52**, 12175–12178.

9 (*a*) Z. T. Ball, Designing Enzyme-like Catalysts: a Rhodium (II) Metallopeptide Case Study, *Acc. Chem. Res.*, 2013, **46**(2), 560–570; (*b*) A. N. Zaykov, B. V. Popp and Z. T. Ball, Helix induction by dirhodium: access to biocompatible metallopeptides with defined secondary structure, *Chem. – Eur. J.*, 2010, **16**, 6651–6659; (*c*) A. N. Zaykov, K. R. MacKenzie and Z. T. Ball, Controlling peptide structure with coordination chemistry: robust and reversible peptide-dirhodium ligation, *Chem. – Eur. J.*, 2009, **15**, 8961–8965; (*d*) J. C. Lewis, Beyond the Second Coordination Sphere: Engineering Dirhodium Artificial Metalloenzymes To Enable Protein Control of Transition Metal Catalysis, *Acc. Chem. Res.*, 2019, **52**, 576–584.

10 S. Pramodini Devi, R. K. Hemakumar Singh, W. Sujata and D. D. Joshi, Synthesis, DNA binding and antimicrobial studies on rhodium(II) complexes of dicyandiamide, *Nucleosides, Nucleotides Nucleic Acids*, 2020, **39**, 923–942.

11 A. Erck, L. Rainen, J. Whileyman, I.-M. Chang, A. P. Kimball and J. Bear, Studies of rhodium(II) carboxylates as potential antitumor agents, *Proc. Soc. Exp. Biol. Med.*, 1974, **145**, 1278–1283.

12 R. A. Howard, A. P. Kimball and J. L. Bear, Mechanism of action of tetra-μ-carboxylatodirhodium(II) in L1210 tumor suspension culture, *Cancer Res.*, 1979, **39**, 2568–2573.

13 J. L. Bear, Rhodium compounds for antitumor use, in *Precious Met. Proc. Jnt. Precious Met. Inst., Conf*, 1986, pp. 337–344.

14 S. A. Hilderbrand, M. H. Lim and S. J. Lippard, Dirhodium tetracarboxylate scaffolds as reversible fluorescence-based nitric oxide sensors, *J. Am. Chem. Soc.*, 2004, **126**, 4972–4978.

15 R. C. Smith, A. G. Tennyson and S. J. Lippard, Polymer-Bound Dirhodium Tetracarboxylate Films for Fluorescent Detection of Nitric Oxide, *Inorg. Chem.*, 2006, **45**, 6222–6226.

16 A. M. Angeles-Boza, P. M. Bradley, P. K. Fu, S. E. Wicke, J. Bacsa, K. R. Dunbar and C. Turro, DNA binding and photocleavage in vitro by new dirhodium(II) dppz complexes: correlation to cytotoxicity and photocytotoxicity, *Inorg. Chem.*, 2004, **43**, 8510–8519.

17 L. E. Joyce, J. D. Aguirre, A. M. Angeles-Boza, A. Chouai, P. K. L. Fu, K. R. Dunbar and C. Turro, Photophysical Properties, DNA Photocleavage, and Photocytotoxicity of a Series of Dppn Dirhodium(II,II) Complexes, *Inorg. Chem.*, 2010, **49**, 5371–5376.

18 K. Sorasaenee, P. K.-L. Fu, A. M. Angeles-Boza, K. R. Dunbar and C. Turro, Inhibition of Transcription in Vitro by Anticancer Active Dirhodium(II) Complexes, *Inorg. Chem.*, 2003, **42**, 1267–1271.

19 H. T. Chifotides, P. K.-L. Fu, K. R. Dunbar and C. Turro, Effect of Equatorial Ligands of Dirhodium(II,II) Complexes on the Efficiency and Mechanism of Transcription Inhibition in Vitro, *Inorg. Chem.*, 2004, **43**, 1175–1183.

20 (*a*) H. T. Chifotides and K. R. Dunbar, Interactions of Metal-Metal-Bonded Antitumor Active Complexes with DNA Fragments and DNA, *Acc. Chem. Res.*, 2005, **38**, 146–156; (*b*) J. D. Aguirre, A. M. Angeles-Boza, C. Turro, J. P. Pellois and K. R. Dunbar, Anticancer activity of heteroleptic diimine complexes of dirhodium: a study of intercalating properties, hydrophobicity and in cellulo activity, *Dalton Trans.*, 2009, **48**, 10806–10812.

21 J. D. Aguirre, A. M. Angeles-Boza, A. Chouai, J. P. Pellois, C. Turro and K. R. Dunbar, Live cell cytotoxicity studies: documentation of the interactions of antitumor active dirhodium compounds with nuclear DNA, *J. Am. Chem. Soc.*, 2009, **131**, 11353–11360.

22 S. U. Dunham, T. S. Remaley, B. S. Moore, D. L. Evans and S. U. Dunham, Isolation, Characterization, and DNA Binding Kinetics of Three Dirhodium(II,II) Carboxyamidate Complexes: $Rh_2(\mu\text{-L})(HNOCCF_3)_3$ where L = $[OOCCH_3]^-$, $[OOCCF_3]^-$, or $[HNOCCF_3]^-$, *Inorg. Chem.*, 2011, **50**, 3458–3463.

23 D. Loreto, A. Esposito, N. Demitri, A. Guaragna and A. Merlino, Reactivity of a fluorine-containing dirhodium tetracarboxylate compound with proteins, *Dalton Trans.*, 2022, **51**, 3695–3705.

24 G. Ferraro, A. Pratesi, L. Messori and A. Merlino, Protein Interactions of Dirhodium Tetraacetate: a Structural Study, *Dalton Trans.*, 2020, **49**, 2412–2416.

25 (*a*) D. Loreto, G. Ferraro and A. Merlino, Unusual Structural Features in the Adduct of Dirhodium Tetraacetate with Lysozyme, *Int. J. Mol. Sci.*, 2021, **22**, 1496; (*b*) D. Loreto and A. Merlino, The Interaction of Rhodium Compounds with Proteins: A Structural Overview, *Coord. Chem. Rev.*, 2021, **442**, 213999.

26 J. D. Aguirre, D. A. Lutterman, A. M. A. Boza, K. R. Dunbar and C. Turro, Effect of Axial Coordination on the Electronic Structure and Biological Activity of Dirhodium(II,II) Complexes, *Inorg. Chem.*, 2007, **46**, 7494–7502.

27 (*a*) L. Trynda and F. Pruchnik, Interaction of Tetra-μ-Acetatodirhodium(II) with Human Serum Albumin, *J. Inorg. Biochem.*, 1995, **58**, 69–77; (*b*) F. Jalilehvand, A. E. Garcia, P. Niksirat, Y. Z. Finfrock and B. S. Gelfand, Binding of histidine and human serum albumin to dirhodium(II) tetraacetate, *J. Inorg. Biochem.*, 2021, **224**, 111556.

28 I. Russo Krauss, G. Ferraro, A. Pica, J. A. Márquez, J. R. Helliwell and A. Merlino, Principles and methods used to grow and optimize crystals of protein–metallodrug adducts, to determine metal binding sites and to assign metal ligands, *Metallomics*, 2017, **9**, 1534–1547.

29 A. Lausi, M. Polentarutti, S. Onesti, J. R. Plaisier, E. Busetto, G. Bais, L. Barba, A. Cassetta, G. Campi, D. Lamba, A. Pifferi, S. C. Mande, D. D. Sarma, S. M. Sharma and G. Paolucci, Status of the crystallography beamlines at Elettra, *Eur. Phys. J. Plus*, 2015, **130**(43), 1–8.

30 C. Vonrhein, C. Flensburg, P. Keller, A. Sharff, O. Smart, W. Paciorek, T. Womack and G. Bricogne, Data Processing and Analysis with the autoPROC Toolbox, *Acta Crystallogr., Sect. D: Biol. Crystallogr.*, 2011, **67**, 293–302.

31 A. J. McCoy, R. W. Grosse-Kunstleve, P. D. Adams, M. D. Winn, L. C. Storoni and R. J. Read, Phaser Crystallographic Software, *J. Appl. Crystallogr.*, 2007, **40**, 658–674.

32 L. Vitagliano, A. Merlino, A. Zagari and L. Mazzarella, Reversible Substrate-Induced Domain Motions in Ribonuclease A, *Proteins*, 2002, **46**, 97–104.

33 J. M. C. Vaney, S. Maignan, M. Ries-Kautt and A. Ducriux, High-resolution Structure (1.33(A) of a HEW Lysozyme Tetragonal Crystal Grown in the APCF Apparatus. Data and Structural Comparison with a Crystal Grown Under Microgravity from SpaceHab-01 Mission, *Acta Crystallogr., Sect. D: Biol. Crystallogr.*, 1996, **52**, 505–517.

34 P. Emsley, B. Lohkamp, W. G. Scott and K. Cowtan, Features and Development of Coot, *Acta Crystallogr., Sect. D: Biol. Crystallogr.*, 2010, **66**, 486–501.

35 G. N. Murshudov, P. Skubák, A. A. Lebedev, N. S. Pannu, R. A. Steiner, R. A. Nicholls, M. D. Winn, F. Long and A. A. Vagin, REFMAC5 for the Refinement of Macromolecular Crystal Structures, *Acta Crystallogr., Sect. D: Biol. Crystallogr.*, 2011, **67**, 355–367.

36 H. Berman, K. Henrickm and H. Nakamura, Announcing the Worldwide Protein Data Bank, *Nat. Struct. Biol.*, 2003, **10**, 980R.

37 P. V. Afonine, R. W. Grosse-Kunstleve, N. Echols, J. J. Headd, N. W. Moriarty, M. Mustyakimov, T. C. Terwilliger, A. Urzhumtsev, P. H. Zwart and P. D. Adams, Towards automated crystallographic structure refinement with phenix.refine, *Acta Crystallogr., Sect. D: Biol. Crystallogr.*, 2012, **68**, 352–367.

38 A. Brink and J. R. Helliwell, Formation of a highly dense tetra-rhenium cluster in a protein crystal and its implications in medical imaging, *IUCrJ*, 2019, **6**, 695–702.

39 G. Ferraro, T. Marzo, T. Infrasca, A. Cilibrizzi, R. Vilar, L. Messori and A. Merlino, A case of extensive protein platination: the reaction of lysozyme with a Pt(II)–terpyridine complex, *Dalton Trans.*, 2018, **47**, 8716–8723.

40 J. R. Helliwell, The crystal structures of the enzyme hydroxymethylbilane synthase, also known as porphobilinogen deaminase, *Acta Crystallogr., Sect. F: Struct. Biol. Commun.*, 2021, **77**, 388–398.

41 Y. Lou, T. P. Remarchuk and E. J. Corey, Catalysis of Enantioselective [2 + 1]-Cycloaddition Reactions of Ethyl Diazoacetate and Terminal Acetylenes Using Mixed-Ligand Complexes of the Series Rh2(RCO2)n(L*4-n). Stereochemical Heuristics for Ligand Exchange and Catalyst Synthesis, *J. Am. Chem. Soc.*, 2005, **127**, 14223–14230.

42 (*a*) L. Messori, T. Marzo, E. Michelucci, I. Russo Krauss, C. Navarro-Ranninger, A. G. Quiroga and A. Merlino, Interaction between anticancer trans-platinum compounds and proteins:crystal structures and ESI-MS spectra of two protein adducts of trans-(dimethylamino)(methylamino) dichloridoplatinum(II)", *Inorg. Chem.*, 2014, **53**(15), 7806–7808; (*b*) M. Serratrice, L. Maiore, A. Zucca, S. Stoccoro, I. Landini, E. Mini, L. Massai, G. Ferraro, A. Merlino, L. Messori and M. A. Cinellu, Cytotoxic properties of a new organometallic platinum(II) complex and its gold(I) heterobimetallic derivatives, *Dalton Trans.*, 2015, **5**(2), 579–590; (*c*) G. Ferraro, D. Loreto and A. Merlino, *Curr. Top. Med. Chem.*, 2021, **21**(1), 6–27.

43 M. Caterino, A. A. Petruk, A. Vergara, G. Ferraro, D. Marasco, F. Doctorovich, D. A. Estrin and A. Merlino, Mapping the protein-binding sites for iridium(iii)-based CO-releasing molecules, *Dalton Trans.*, 2016, **45**(30), 12206–12214.

44 L. Messori, F. Scaletti, L. Massai, M. A. Cinellu, I. Russo Krauss, G. di Martino, A. Vergara, L. Paduano and A. Merlino, Interactions of Gold-based drugs with proteins: crystal structure of the adduct formed between Ribonuclease A and a cytotoxic gold(III) compound, *Metallomics*, 2014, **6**(2), 233–236.

45 A. Vergara, D. Montesarchio, I. Russo Krauss, L. Paduano and A. Merlino, Investigating the ruthenium metallation of proteins: X-ray structure and Raman microspectroscopy of the complex between RNase A and AziRu, *Inorg. Chem.*, 2013, **52**(19), 10714–10716.

46 (*a*) A. Vergara, G. D'Errico, D. Montesarchio, G. Mangiapia, L. Paduano and A. Merlino, Interaction of anticancer Ruthenium compounds with proteins: High resolution X-ray structures and Raman microscopy studies of the adduct between hen egg white lysozyme and AziRu, *Inorg. Chem.*, 2013, **52**(8), 4157–4159; (*b*) L. Chiniadis, P. Giastas, I. Bratsos and A. Papakyriakou, Insights into the Protein Ruthenation Mechanism by Antimetastatic Metallodrugs: High-Resolution X-ray Structures of the Adduct formed between Hen Egg-White Lysozyme and NAMI-A at Various Time Points, *Inorg. Chem.*, 2021, **60**(14), 10729–10737.

47 (*a*) L. Messori, F. Scaletti, L. Massai, M. A. Cinellu, C. Gabbiani, A. Vergara and A. Merlino, The Mode of Action of Anticancer Gold-Based Drugs: a Structural Perspective, *Chem. Commun.*, 2013, **49**(86), 10100–10102; (*b*) I. Russo Krauss, L. Messori, M. A. Cinellu, D. Marasco, R. Sirignano and A. Merlino, Interactions of Gold-based Drugs with Proteins: the structure and stability of the Adduct Formed in the reaction between Lysozyme and the Cytotoxic Gold(III) Compound Auoxo3, *Dalton Trans.*, 2014, **43**(46), 17483–17488; (*c*) A. Merlino, M. Caterino, I. Russo Krauss and A. Vergara, Missing gold atoms in crystals of lysozyme used to grow gold nanoparticles, *Nat. Nanotechnol.*, 2015, **4**, 285.

48 M. J. Panzner, S. M. Bilinovich, W. J. Youngs and T. C. Leeper, Silver metallation of hen egg white lysozyme: X-ray crystal structure and NMR studies, *Chem. Commun.*, 2011, **47**(46), 12479–12481.

49 (*a*) L. Messori, T. Marzo, C. Gabbiani, A. Alvarez-Valdes, A. Quiroga and A. Merlino, Peculiar features in the crystal structure of the adduct formed between cis-PtI2(NH3)2 and

hen egg white lysozyme, *Inorg. Chem.*, 2013, **52**(24), 13827–13829; (*b*) D. Marasco, L. Messori, T. Marzo and A. Merlino, Oxaliplatin vs Cisplatin: competition experiments on their binding to Lysozyme, *Dalton Trans.*, 2015, **44**, 10392–10398.

50 A. A. Petruk, A. Vergara, D. Marasco, D. Bikiel, F. Doctorovich, D. A. Estrin and A. Merlino, Interaction between proteins and Iridium-based CO releasing molecules: mechanism of adduct formation and CO release, *Inorg. Chem.*, 2014, **53**(19), 10456–10462.

51 (*a*) S. L. Binkley, T. C. Leeper, R. S. Rowlett, R. S. Herrick and C. J. Ziegler, Re(CO)3(H_2O)3+ binding to lysozyme: structure and reactivity, *Metallomics*, 2011, **3**, 909–916; (*b*) F. Zobi and B. Spingler, Post-protein-binding reactivity and modifications of the fac-[Re(CO)3]+ core, *Inorg. Chem.*, 2012, **51**, 1210–1212.

52 M. P. Sullivan, M. K. Nieuwoudt, G. A. Bowmaker, N. Y. S. Lam, D. Truong, D. C. Goldstone and C. G. Hartinger, Unexpected arene ligand exchange results in the oxidation of an organoruthenium anticancer agent: the first X-ray structure of a protein-Ru(carbene) adduct, *Chem. Commun.*, 2018, **54**, 6120–6123.

53 (*a*) L. Messori and A. Merlino, Ruthenium metalation of proteins: the X-ray structure of the complex formed between NAMI-A and hen egg white lysozyme, *Dalton Trans.*, 2014, **43**, 6128–6131; (*b*) L. Messori, T. Marzo, R. N. Fernandes Sanches, H.-U. Rehman, D. de Oliveira Silva and A. Merlino, Unusual Structural Features in the Lysozyme Derivative of Tetrakis(acetato)chlorido Diruthenium(II,III) Complex, *Angew. Chem., Int. Ed.*, 2014, **53**(24), 6172–6175; (*c*) H. Tabe, K. Fujita, S. Abe, M. Tsujimoto, T. Kuchimaru, S. Kizaka-Kondoh, M. Takano, S. Kitagawa and T. Ueno, Preparation of a Cross-Linked Porous Protein Crystal Containing Ru Carbonyl Complexes as a CO-Releasing Extracellular Scaffold, *Inorg. Chem*, 2015, **54**, 215–220; (*d*) J. D. Seixas, M. F. A. Santos, A. Mukhopadhyay, A. C. Coelho, P. M. Reis, L. F. Veiros, A. R. Marques, N. Penacho, A. M. L. Gonçalves, M. J. Romão, G. J. L. Bernardes, T. Santos-Silva and C. C. Romão, A Contribution to the Rational Design of Ru(Co)3Cl2L Complexes for in Vivo Delivery of CO, *Dalton Trans.*, 2015, **44**, 5058–5075.

54 R. Mizutani, Y. Shimizu, R. Saiga, G. Ueno, Y. Nakamura, A. Takeuchi, K. Uesugi and Y. Suzuki, Spatiotemporal development of soaked protein crystals, *Sci. Rep.*, 2014, **4**, 5731–5731.

55 J. Telser and R. S. Drago, Reactions of Rhodium Trifluoroacetate with Various Lewis Bases. Formation of 4 : 1 Complexes with Pyridine and tert-Butyl Isocyanide and Rhodium-Rhodium Bond Cleavage with Phosphorus Donors, *Inorg. Chem.*, 1984, **23**, 2599–2606.

56 T. R. Webb and T.-Y. Dong, Some observations on solution chemistry of Molybdenum(II) trifluoroacetate, *Inorg. Chem.*, 1982, **21**, 114–116.